Comparative Analysis of Lattice-based All-Pass Filter and Second Order Generalized Integrator as Orthogonal System Generator of a PLL

Luciano Emilio BELANDRIA[1], *Nancy Alejandra AGUDELO*[1], *Joan BERGAS-JANE*[2]

[1]Department of Electronic Engineering, National Experimental University of Tachira, Universidad, 5001 San Cristobal, Venezuela
[2]Center of Technological Innovation in Static Converters and Drives, Department of Electrical Engineering, Polytechnic University of Catalonia, Diagonal 647, 08028 Barcelona, Spain

lbeland@unet.edu.ve, agudeloalejandra24@gmail.com, joan.gabriel.bergas@upc.edu

DOI: 10.15598/aeee.v19i1.4002

Article history: Received Nov 13, 2020; Revised Jan 31, 2021; Accepted Feb 10, 2021; Published Mar 31, 2021.

Abstract. *This paper presents a steady-state comparison of two methods that generate an orthogonal voltage system for a single-phase Phase-Locked Loop (PLL) structure: a widely accepted one based on a Second Order Generalized Integrator (SOGI) and a new one based on a All-Pass Filter (APF) with Lattice structure. Both methods are very attractive because of their simple digital implementation, low computational load and good performance under harmonically distorted grid conditions and variable frequency, so they are a good alternative to other known methods. The paper derives and analyzes the full state space models of the two methods. It is shown that these two methods are equivalent in the most common operation conditions of distributed energy resources, although the APF structure is clearly better than the SOGI one because it maintains its orthogonal generation ability for any higher notch frequencies and any lower sampling frequencies. The comparative analysis were validated by simulation using MATLAB/Simulink and experimental results using a fixed-point DSP.*

Keywords

All-Pass Filter, Orthogonal Signal Generator, Phase-Locked Loop, Single-Phase PLL, Notch Filter, Second Order Generalized Integrator.

1. Introduction

The use, development and deployment of Distributed Energy Resources (DERs), especially renewable resources, has increased dramatically in the last decade. This is changing the paradigm of electric generation [1], [2], [3], and [4]. Single-phase grid-connected inverters are found in many DERs, such as photovoltaic inverters and energy storage devices [5] and [6].

Inverter system control must ensure that the power generation system is synchronized with the grid, and that phase angle jumps are detected for reliable power delivery [7] and [8]. Moreover, it must ensure that grid-connected system performance complies with operation requirements under the most common distortions, such as line harmonics, notches, voltage dips, rises and falls, and frequency variations.

Phase, frequency and amplitude characterize the single-phase grid voltage signal and knowledge of these parameters is fundamental in the design of grid-connected inverter systems [9], like the one in Fig. 1. In order to meet the new requirements of network codes and optimize inverter performance, a PLL is used for rapid synchronization with the grid.

The main task of the PLL is to accurately detect the actual voltage phase angle at the Point of Common Coupling (PCC), even in the presence of voltage harmonics and unbalance [10] and [11]. This structure, for example, should be used to provide any unity power factor operation which involves synchronization of the

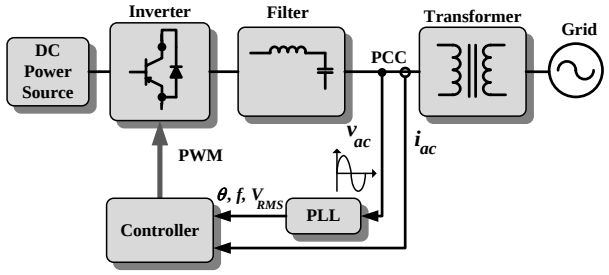

Fig. 1: Grid-connected power conversion systems.

inverter output current with the grid voltage and to give a clean sinusoidal current reference, among other functions.

For three-phase applications, some of the recent and most popular grid synchronization techniques for detecting the phase and frequency of the mains voltage signal using PLL are presented in [12], where a complete study was carried out on the control strategies of Distributed Generation Power Systems (DGPSs) under ideal and non-ideal network conditions. These techniques are: basic structure traditional Synchronous Reference Frame PLL (SRF-PLL), Enhanced PLL (EPLL), Dual Second Order Generalized Integrator PLL (DSOGI-PLL), Moving Average Filter (MAF) and Decoupled Double Synchronous Reference (DDSRF).

Indeed, the single-phase structure of PLLs limits the use of some well-known three-phase control strategies [13] and [14]. In single-phase systems, less is known about the network operating conditions than in three-phase systems. That is why the most advanced methods used to overcome this limitation must create an orthogonal voltage system [15] and then exploit the existing three-phase control methods. In this line of research, several advanced PLL techniques, have been proposed for single-phase applications [16], [17], [18], and [19].

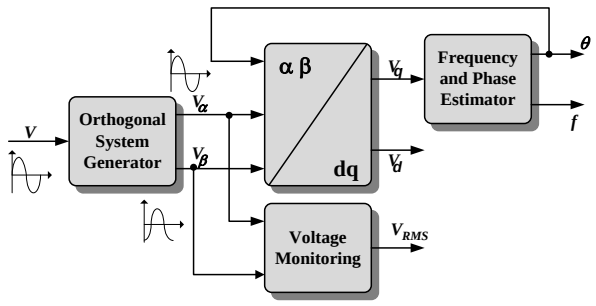

Fig. 2: PLL using the park transformation.

General structure of a single-phase PLL algorithm based on Orthogonal Signal Generator (OSG), also called Quadrature Signal Generator (QSG), for grid synchronization is presented in [15], [16], [20], [21], [22], [23], and [24]. This structure can use the Park Transformation, as shown in Fig. 2 or the arc-tangent function depicted in Fig. 3. The main difference between OSG-based single-phase PLLs lies in the way orthogonal voltage systems are generated.

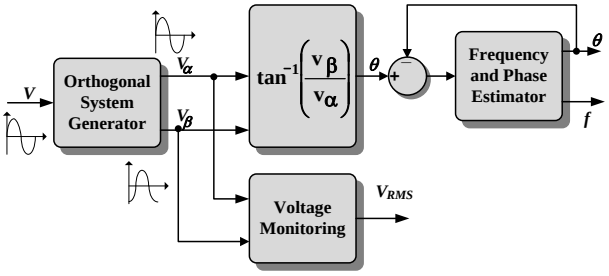

Fig. 3: PLL using the arctangent function.

The OSG-based single-phase PLL structures, Fig. 2 and Fig. 3, found in the state-of-the-art methods are basically formed by two blocks. In the first, an orthogonal system in phase with the above signal is generated from a single reference sinusoidal signal. The second block uses either a feedback loop through the $\alpha\beta$ to dq transformation or the arc-tangent function to determine the phase angle of the reference signal.

The methods for OSG of a single-phase PLL must be easy to apply in practice. Moreover, the OSG must deliver the filtered output without any delay, because of its resonance at the fundamental frequency, not to be affected by frequency changes. The most common methods used in the literature to generate the orthogonal voltage are presented in [15], [19], [20], [21], [25], [26], [27], [28], [29], [30], [31], and [33]. One using a block of a Transport Delay function is shown in Fig. 4. It introduces a 90 degree phase shift with respect to the input signal [21] and [28]. Another method uses the Hilbert Transformation [29], depicted in Fig. 5, and the Inverse Park Transformation [19], [30], and [31], shown in Fig. 6. However, these methods have one or more of the following deficiencies: frequency dependence, high complexity, non-linearity, and poor or no filtration.

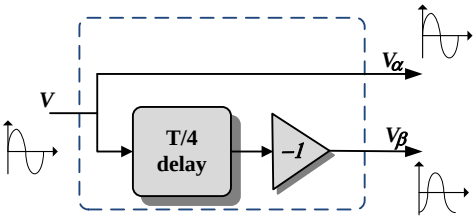

Fig. 4: Transport delay function.

To improve the deficiencies mentioned in the OSG methods, an improved Average Filter (AF) is proposed in [32], with a simple structure and implementation, which, integrated into OSG, attenuates the negative effect of voltage harmonics and unbalances on orthogonal

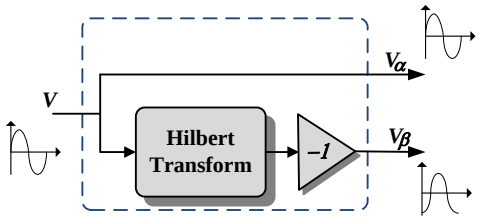

Fig. 5: Hilbert transformation.

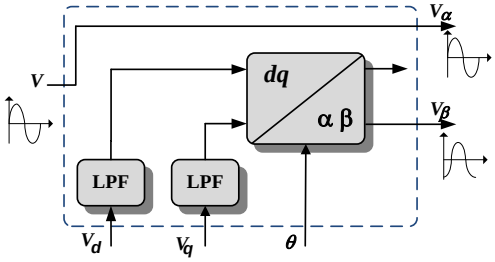

Fig. 6: Inverse park transformation.

d-q signals for PLL. Providing fast phase detection and fast dynamic response without using the second order filters, which reduce the dynamic response time and the detection of the synchronization unit.

In [34], a Frequency Lock Loop (FLL) with a Generalized Integrator (GI) was proposed. In the GI-FLL, the GI part is a OSG, while the FLL part uses the signals generated for unknown frequency estimation purposes. The GI works as an adaptive bandpass filter using coordinate transformation, which allows to improve the dynamic tuning range, with an excellent balance between the convergence speed and the maximum acceptable peak estimation error, but with some computational cost additional to that needed for accuracy and the FLL has to add the normalization of the gain that the GI does not have.

The technique using the grid voltage demodulation to obtain a OSG is proposed in [35], in a Demodulation Type PLL (DT-PLL) with improved DC offset rejection capacity, for the adaptive estimation of the phase angle and the frequency of a single-phase system, which avoids the use of any low-pass filter. The demodulation has good dynamic performance and disturbance rejection ability. However, due to the presence of trigonometric quantities in the estimator dynamics, small-signal modelling-based parameter tuning can be complicated for DT-PLL. Moreover, real-time implementation of trigonometric functions is computationally expensive.

A single-phase PLL structure based on SOGI which overcomes the above problems and avoidance of filtering delays due to its resonance at the fundamental frequency was presented in [15], [20], [21], [36], [37], [38], [39], [40], and [41]. Thus, the way in which the two signals are generated is improved. In [42], [43], and [44] a three-phase PLL structure based on a Double Second Order Generalized Integrator (DSOGI) is presented.

The SOGI structure has also been applied to other aspects of power electronic control, especially in the current control loop [37] and [38], detection of harmonics [39] and active anti-islanding methods [22].

However, as already indicated in [15], [37], and [38], the SOGI was designed in the continuous time and quadrature phase delay and amplitude ripples are present in its discrete application. Moreover, it is difficult to apply this structure on a fixed-point DSP or FPGA due to their limited precision and sensitivity to coefficient rounding.

A second-order APF with Lattice structure was proposed in [45], [46], [47], [48], [49], and [50]. This filter generates orthogonal signals necessary for the PLL, with good noise filtering capability but amplitudes different from that of the single-phase input signal. Here a APF with Lattice structure is proposed as OSG which meets all requirements and overcomes all the drawbacks of the methods used in single-phase PLL while maintaining any unity gain with respect to the input.

This paper performs a comparative steady-state analysis of the structures based on APF and SOGI as part of a PLL. These structures are widely used for filtering the power supply signal to ensure the best possible synchronization system references for use in single-phase converters operating in highly disturbed environments. Solutions for the discrete application of the two structures are also provided. Simulations and a fixed-point DSP implementation validate the effectiveness of one or another structure.

The rest of the paper is organized as follows. Section 2. describes the lattice APF as OSG with its main diagrams and equations. In Sec. 3. , the SOGI algorithm is presented. Section 4. provides discrete time simulation results for both OSGs using as input a 50 Hz normalized sinusoidal signal in both filters. In Sec. 5. , the experimental results of a fixed-point DSP implementation of both OSGs under the same simulation conditions are discussed. Finally, Sec. 6. draws the conclusions.

2. Lattice-Based APF

In the approach proposed in [49], no unity gain has been considered while, in this paper, a new structure of OSG based on APF, as illustrated in Fig. 7, is proposed characterized by unity gain [50].

In the system, the output signals $x_1(n)$ and $x_2(n)$ have a -90 degree and 0 phase shift, respectively,

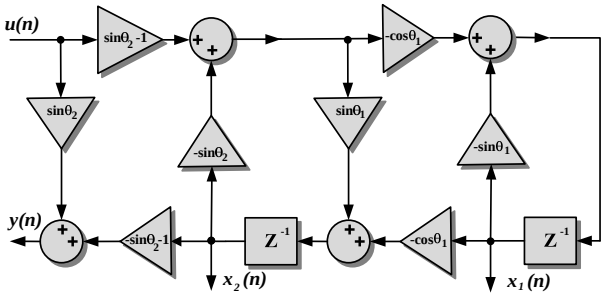

Fig. 7: APF as OSG with unity gain.

with respect to the input signal with unity gain, are defined as:

$$x_1(n) = \frac{\cos\theta_1(1-\sin\theta_2)z^{-1}}{1+\sin\theta_1(1+\sin\theta_2)z^{-1}+\sin\theta_2 z^{-2}}u(n), \tag{1}$$

$$x_2(n) = \frac{\sin\theta_1(\sin\theta_2-1)z^{-1}+(\sin\theta_2-1)z^{-2}}{1+\sin\theta_1(1+\sin\theta_2)z^{-1}+\sin\theta_2 z^{-2}}u(n). \tag{2}$$

The space-state equation of the APF with Lattice structure can be obtained from the system in Fig. 7, is defined as:

$$\begin{bmatrix} x_1(n+1) \\ x_2(n+1) \\ y(n) \end{bmatrix} = \\ = \begin{bmatrix} -\sin\theta_1 & \cos\theta_1\sin\theta_2 & \cos\theta_1(1-\sin\theta_2) \\ -\cos\theta_1 & -\sin\theta_1\sin\theta_2 & \sin\theta_1(\sin\theta_2-1) \\ 0 & -(1+\sin\theta_2) & \sin\theta_2 \end{bmatrix} \cdot \begin{bmatrix} x_1(n) \\ x_2(n) \\ u(n) \end{bmatrix}, \tag{3}$$

where θ_1 is associated with the notch frequency ω_0, at which the APF offers a phase shift of π radians, and θ_2 is associated with the 3 dB attenuation Bandwidth BW of the filter. They are defined as:

$$\theta_1 = \frac{\omega_0}{f_s} - \frac{\pi}{2}, \tag{4}$$

$$\theta_2 = \arcsin\left(\frac{1-\tan\left(\frac{BW}{2}\right)}{1+\tan\left(\frac{BW}{2}\right)}\right), \tag{5}$$

$$BW = \frac{2\pi B}{f_s}, \tag{6}$$

where f_s and B correspond to the sampling frequency and bandwidth in Hz, respectively. Independent adjustment of notch frequency and bandwidth is a desirable attribute. Adjusting the bandwidth for any sampling frequency from Eq. (6), either directly or adaptively, allows the APF to reject very low frequencies, even rejecting the DC offset, without adding another type of filter and without interfering with the tuning frequency. This feature of the APF can comply with those of the OSG with DC offset rejection capability proposed in [33], with only the adjustment of a single parameter.

The structure in Fig. 7, is theoretically stable and numerically well behaved in time-varying environments [49]. Each rotation angle ω_k(k = 1, 2) is directly controlled, so that θ_1 and θ_2 are converted into the adjustable parameters for adaptive performance. Elements **A** and **B** of the structure are extracted from Eq. (3):

$$\mathbf{A} = \begin{bmatrix} -\sin\theta_1 & \cos\theta_1\sin\theta_2 \\ -\cos\theta_1 & -\sin\theta_1\sin\theta_2 \end{bmatrix}, \tag{7}$$

$$\mathbf{B} = \begin{bmatrix} \cos\theta_1(1-\sin\theta_2) \\ -\sin\theta_1(1-\sin\theta_2) \end{bmatrix}. \tag{8}$$

Figure 8, shows the Bode diagram of the APF as normalized OSG for a tuning frequency of 50 Hz.

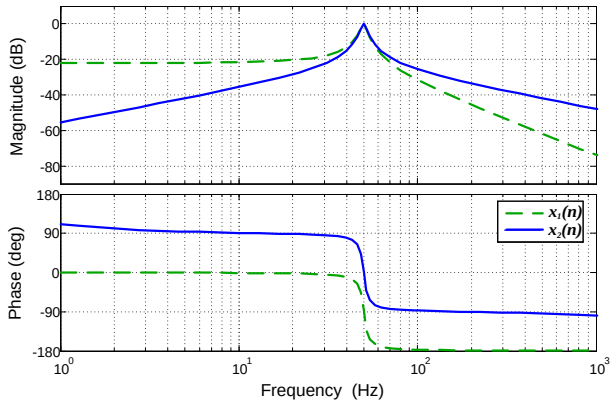

Fig. 8: Bode diagram of lattice-based APF as normalized OSG.

3. The SOGI

A SOGI is equivalent to two Proportional-Integral (PI) controllers in synchronous reference frames compensating the sequences of positive and negative [15], [20], [37], [38], [39], and [40].

SOGI is proposed to obtain a zero steady state error using sinusoidal references working on the $\alpha\beta$ stationary reference frame. This method has been included in harmonic elimination algorithms (because harmonics act in a very narrow band around their resonance frequency); grid sequence detection and quadrature signal generation algorithms; algorithms for converter synchronization to the power supply; and for multi-frequency detection.

The transfer function of a SOGI for a single sinusoidal signal is [37] and [38]:

$$G(s) = \frac{2s}{s^2+\omega_0^2}, \tag{9}$$

where ω_0 is the resonance frequency and s the Laplace operator. The integrator output contains not

only the integrated input but also an insignificant additional component. In order to use them to generate quadrature signals, the original topology is modified, as shown in Fig. 9. The resulting mathematical expression is:

$$G(s) = \frac{x(s)}{y(s)} = \frac{\omega_0 s}{s^2 + \omega_0^2}. \tag{10}$$

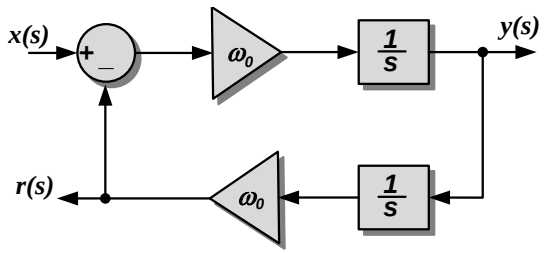

Fig. 9: Continuous-time SOGI.

The new transfer function has two poles at $\pm j\omega_0$ and a zero at the origin, just as Eq. (9). The only difference between the two expressions is in the gain, which is not significant as far as the final performance is concerned. However, the function leads to a more general structure that can be used for both power converters control and synchronization tasks.

The SOGI structure for generation of orthogonal signals, also known as OSG-SOGI, is outlined in Fig. 10. As can be seen, the basic element is a SOGI [15], [20], [37], [38], [39], and [40]. The continuous-time transfer functions are:

$$\frac{v'(s)}{v(s)} = \frac{K_s \omega_0 s}{s^2 + K_s \omega_0 s + \omega_0^2}, \tag{11}$$

$$\frac{qv'(s)}{v(s)} = \frac{K_s \omega_0^2}{s^2 + K_s \omega_0 s + \omega_0^2}. \tag{12}$$

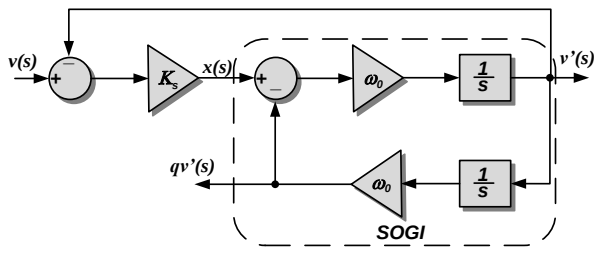

Fig. 10: Continuous-time OSG-SOGI.

Discrete-time implementation of the SOGI can be accomplished by discretizing the continuous-time transfer functions or by using discrete integrators [15], [37], and [38].

Figure 11 shows the discrete-time SOGI structure. Its output behaves like that of the continuous-time SOGI in Fig. 9 upon application of a step signal of amplitude 1 at input $x(n)$, that is a sinusoidal signal of pulsation ω_0 and amplitude 1. The choice of this SOGI is based on the use of discrete Euler Backward Integrator with computational delay added in series with the feedback gain, modeling the inherent delay caused by the programming process. Moreover, its structure is more similar to that of the classical PI controller.

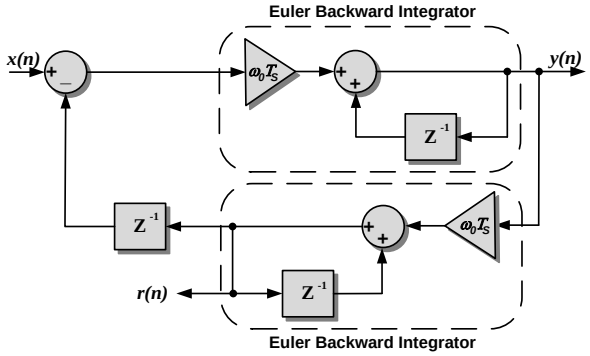

Fig. 11: SOGI based on Euler Backward Integrator and computational delay.

The transfer function of the discrete-time SOGI is:

$$G(z) = \frac{\omega_0 T_s - \omega_0 T_s z^{-1}}{1 + (\omega_0^2 T_s^2 z^{-1} - 2) + z^{-2}}. \tag{13}$$

Figure 12 displays the SOGI based on discrete Euler Backward Integrator within an OSG-SOGI, which ensures that signals v' and qv' are quadrature signals at all operating frequencies. The OSG-SOGI allows independent adjustment of the notch frequency ω_0 and of the 3 dB attenuation bandwidth BW, considering the sampling period T_s, according to:

$$K_t = \omega_0 T_s, \tag{14}$$

$$K_s = \frac{BW}{\omega_0}\sqrt{0.98}. \tag{15}$$

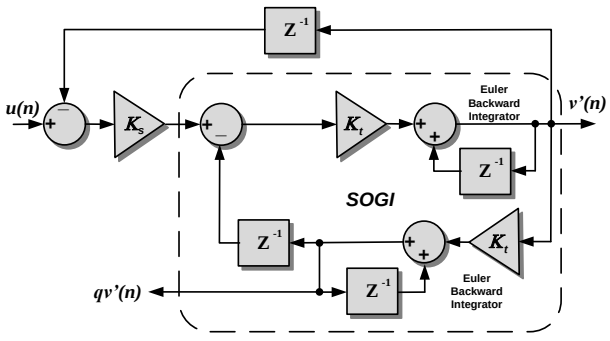

Fig. 12: Discrete-time OSG-SOGI structure.

The OSG-SOGI can also be expressed by state equation form based on the final circuit of Fig. 13, which is equivalent to that of Fig. 12, where $x_1(n)$ and $x_2(n)$ are the signals corresponding to the orthogonal system and are denoted as in the APF, with a -90 and 0 degree phase shift, respectively, and unity gain with respect to the input signal of power $u(n)$ at instant n.

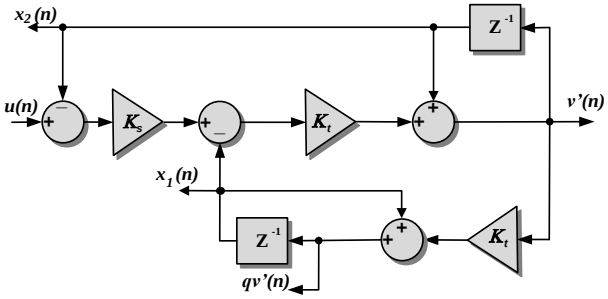

Fig. 13: Definitive OSG-SOGI structure.

This orthogonal system is given by:

$$x_1(n) = \\ = \frac{K_s K_t^2 z^{-1}}{1 + (K_s K_t - 2 + K_t^2) z^{-1} + (1 - K_s K_t) z^{-2}} u(n), \tag{16}$$

$$x_2(n) = \\ = \frac{K_s K_t z^{-1} - K_s K_t z^{-2}}{1 + (K_s K_t - 2 + K_t^2) z^{-1} + (1 - K_s K_t) z^{-2}} u(n). \tag{17}$$

Figure 14 offers the Bode diagram of the OSG-SOGI, for a tuning frequency of 50 Hz. Considering that outputs $x_1(n+1)$ and $x_2(n+1)$ are the same answers *qv'(n)* and *v'(n)*, the state equation is:

$$\begin{bmatrix} x_1(n+1) \\ x_2(n+1) \\ y(n) \end{bmatrix} = \\ = \begin{bmatrix} 1 - K_t^2 & K_t(1 - K_s K_t) & K_s K_t^2 \\ -K_t & 1 - K_s K_t & K_s K_t \\ 0 & 1 & 0 \end{bmatrix} \cdot \begin{bmatrix} x_1(n) \\ x_2(n) \\ u(n) \end{bmatrix}. \tag{18}$$

Elements **A** and **B** of the structure can be extracted from Eq. (18):

$$\mathbf{A} = \begin{bmatrix} 1 - K_t^2 & K_t(1 - K_s K_t) \\ -K_t & 1 - K_s K_t \end{bmatrix}, \tag{19}$$

$$\mathbf{B} = \begin{bmatrix} K_s K_t^2 \\ K_s K_t \end{bmatrix}. \tag{20}$$

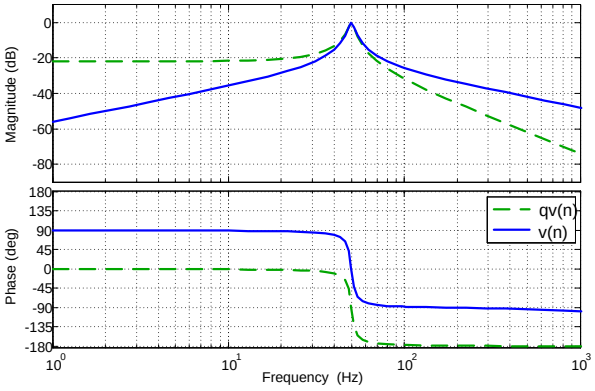

Fig. 14: Bode diagram of the OSG-SOGI.

4. Behavior and Comparison of OSGs

The structures of the lattice-based APF in Fig. 7 and the OSG-SOGI in Fig. 13 can be easily implemented as matrix system consisting of elements **A** and **B** only, thus we will have the equation of state of the form:

$$\begin{bmatrix} x_1(n+1) \\ x_2(n+1) \end{bmatrix} = \begin{bmatrix} \mathbf{A} & \mathbf{B} \end{bmatrix} \cdot \begin{bmatrix} x(n) \\ u(n) \end{bmatrix}. \tag{21}$$

Both structures have the ability to generate, in phase with the input signal, an orthogonal system. Figure 15 shows the implementation of the lattice-based APF and OSG-SOGI structures in state equation. Two parameters identified as $x_1(n)$ and $x_2(n)$, which constitute the orthogonal system, are observed.

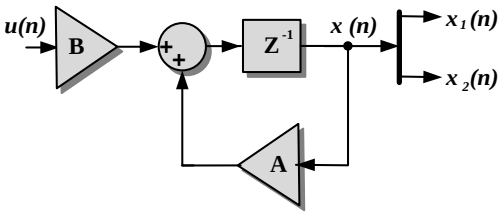

Fig. 15: OSG in state equation.

Both structures are simulated under the same conditions to compare them as Band-Pass Filters (BPF) which generate a disturbance-free orthogonal system with one signal image of the fundamental input signal and another one delayed 90 degrees with respect to the same input signal. The two filters are evaluated using any unity amplitude sinusoidal signal at the frequency of 50 Hz as the fundamental input signal. Is sets a sampling frequency of 20 kHz, 50 Hz tuning frequency and a low bandwidth of 4 Hz, narrow enough for many applications where a very selective magnitude response is required, with a high quality factor. The simulation is implemented in MATLAB/Simulink. The state equa-

tion from Eq. (3) for the APF with the values estimated under these conditions is:

$$\begin{bmatrix} x_1(n+1) \\ x_2(n+1) \end{bmatrix} = \\ = \begin{bmatrix} 0.9998766 & 0.0156876 & 0.0000197 \\ -0.0157073 & 0.9986209 & 0.0012557 \end{bmatrix} \cdot \begin{bmatrix} x_1(n) \\ x_2(n) \\ u(n) \end{bmatrix}. \quad (22)$$

And the state equation from Eq. (18) for the OSG-SOGI with the values estimated:

$$\begin{bmatrix} x_1(n+1) \\ x_2(n+1) \end{bmatrix} = \\ = \begin{bmatrix} 0.9997532 & 0.0156884 & 0.0000195 \\ -0.0157080 & 0.9987560 & 0.0012440 \end{bmatrix} \cdot \begin{bmatrix} x_1(n) \\ x_2(n) \\ u(n) \end{bmatrix}. \quad (23)$$

Figure 16 gives the frequency response for outputs $x_2(n)/u(n)$, of Eq. (2) and Eq. (17), corresponds to the APF and the OSG-SOGI. For frequencies over 10 Hz both structures maintain a strong similarity in both magnitude and phase. But for frequencies below 10 Hz they already begin to differentiate, the APF begins to increase its phase to values greater than 90 degrees. For frequencies below 1 Hz the difference in magnitude begins to be more noticeable.

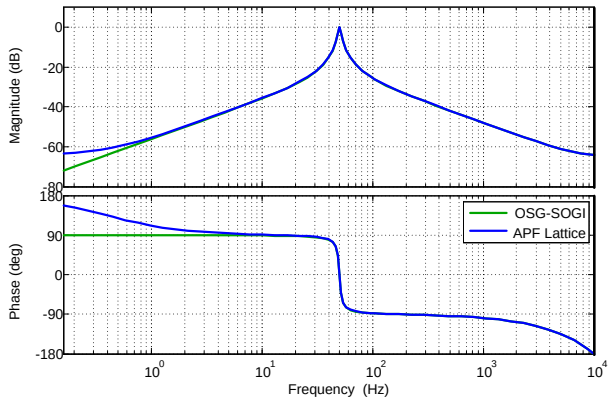

Fig. 16: Bode diagram of $x_2(n)/u(n)$ in Lattice-based APF and OSG-SOGI.

As shown in Eq. (22) and Eq. (23), the values of the coefficients of both filters are nearly identical under these operating conditions, the differences between the coefficients are less than 0.0001233. Hence, their frequency responses should have a very similar behavior.

The frequency responses are obtained for $x_2(n)/u(n)$, in the APF and in the OSG-SOGI for a range of fundamental frequencies, from 100 Hz to 10 kHz, with a bandwidth of 4 Hz, a sampling frequency of 20 kHz, for both filters. In Fig. 17, one can observe that both OSG behave like a BPF, but for fundamental frequencies greater than 400 Hz, the magnitude responses begin to have differences, although they maintain their tuning. From frequencies greater than 3 kHz, the SOGI begins to lose its tuning, both in its magnitude and phase response.

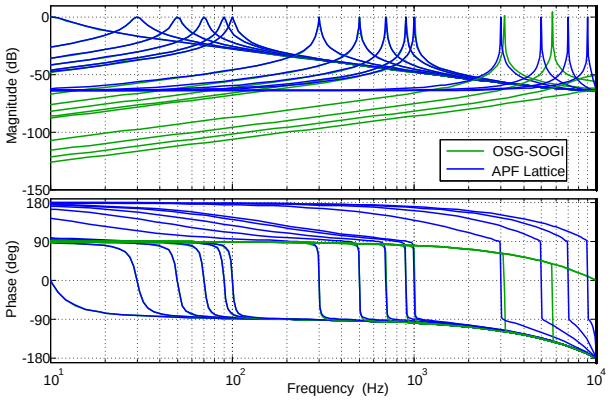

Fig. 17: Bode diagram of $x_2(n)/u(n)$ in Lattice-based APF and OSG-SOGI for various tuning frequencies.

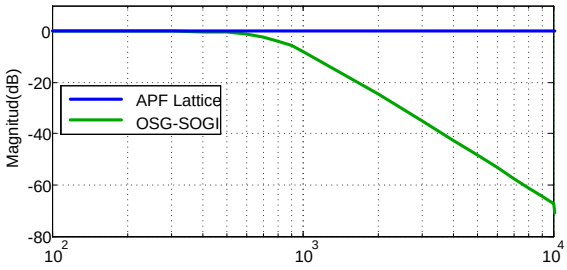

(a) For various tuning frequencies.

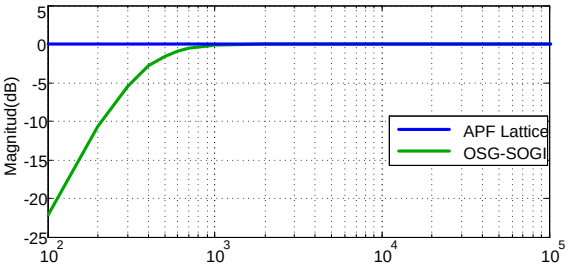

(b) For various sampling frequencies.

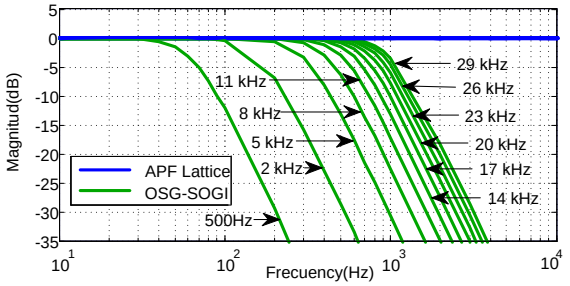

(c) For various sampling frequencies and variation of the tuning frequency.

Fig. 18: Magnitude of $x_2(n)/u(n)$ in the Lattice-based APF and OSG-SOGI.

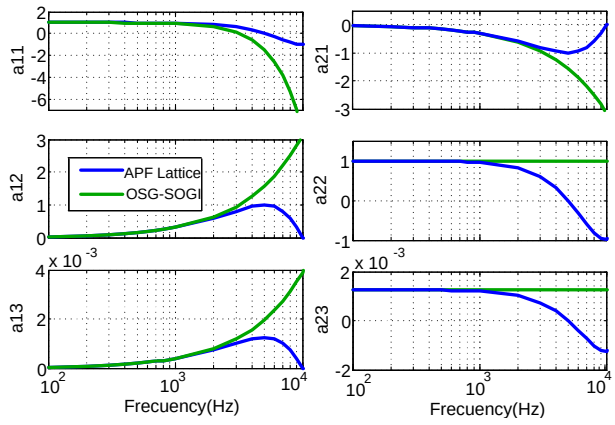

(a) For various tuning frequencies.

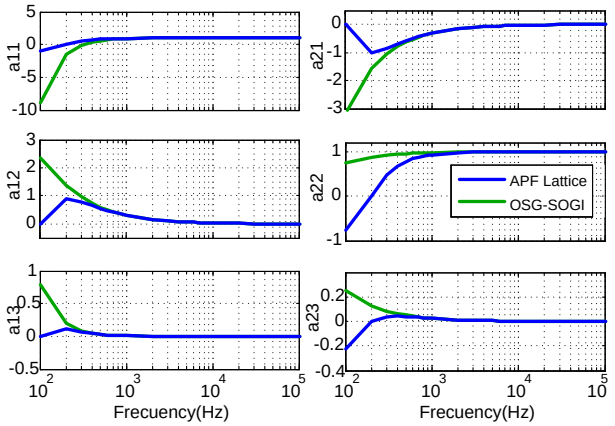

(b) For various sampling frequencies.

Fig. 19: Behavior of the matrix parameters of the state equation of APF and OSG-SOGI.

Figure 18 displays the result of the magnitude for $x_2(n)/u(n)$ of the lattice APF and the OSG-SOGI with a bandwidth of 4 Hz and a sampling frequency of 20 kHz at various frequencies, for a tuning frequency of 50 Hz with sampling frequencies ranging from 100 Hz to 100 kHz and for various sampling frequencies and variations of the frequency of tuning. As can be noticed, from a tuning frequency of 600 Hz and a sampling frequency below 1 kHz, the tuning of the SOGI is not accurate, and so are its characteristics as OSG, which does not happen with the APF.

The magnitude in dB of $x_2(n)/u(n)$ is obtained by evaluating the APF and the OSG-SOGI with a bandwidth of 4 Hz, depicted in Fig. 18(a) for a sampling frequency of 20 kHz and the variation of the tuning frequency. In Fig. 18(b) the tuning frequency is kept at 50 Hz with variation of the sampling frequency from 100 Hz to 100 kHz and in Fig. 18(c) the result of the magnitude is shown for several sampling frequencies (500 Hz, 2 kHz, 5 kHz, 8 kHz, 11 kHz, 14 kHz, 17 kHz, 20 kHz, 23 kHz, 26 kHz, and 29 kHz) and variation of the tuning frequency. As can be seen, the APF maintains a constant magnitude of 0 dB for all the variations in all the evaluated ranges. On the other hand, the SOGI loses the tuning starting from a tuning frequency of 500 Hz and a sampling frequency lower than 1 kHz, and therefore hence its characteristics as OSG.

Figure 19 shows the behavior of the matrix parameters of the state equation of the APF Eq. (3) and the OSG-SOGI Eq. (18) for various tuning and sampling frequencies. The parameters begin to differ more significantly from tuning frequencies greater than 500 Hz and sampling frequencies below 1 kHz in most cases. This is demonstrated by the results in Fig. 16, Fig. 17, and Fig. 18.

Figure 20, has the magnitude response surface for $x_2(n)/u(n)$, as a function of the tuning frequency and the sampling frequency. Observing that for the APF, the result is a completely flat surface with a magnitude of 0 dB constant for any variation of the frequencies. This does not occur for the OSG-SOGI, where it is observed that the magnitude response varies as the frequencies vary, moving away from the required passband. Being the worst case when the tuning frequency increases and the sampling frequency decreases.

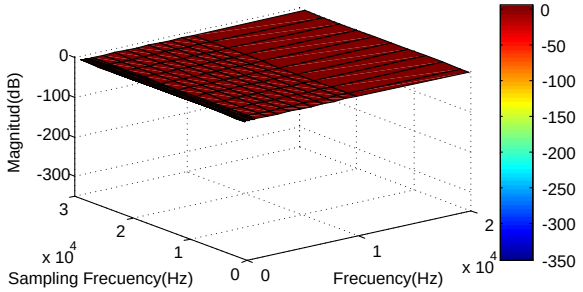

(a) APF.

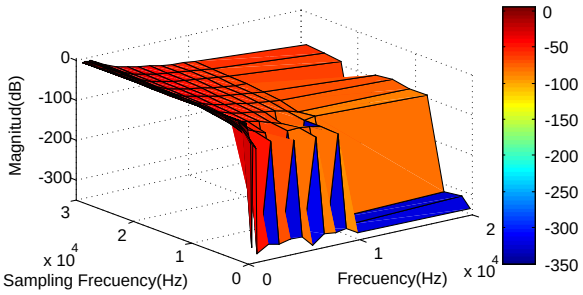

(b) OSG-SOGI.

Fig. 20: Surface of the magnitude of $x_2(n)/u(n)$ for various sampling frequencies and variation of the tuning frequency.

5. Simulation and Experimental Results

In order to validate the analysis, the APF and the OSG-SOGI are simulated by using MATLAB/Simulink program and an experimental setup was implemented. A CDM2480 test platform, with a TMS320F2812 fixed-point DSP from Texas Instruments as the central element, suitable for motion control and power electronics applications, was used to implement and test both structures as OSG. The fixed point DSP, with a clock frequency of 150 MHz, was used to generate the input signal, the OSG algorithms and the output signals with a 12 bit D/A converter.

All simulated and experimental results, were obtained using the structures in Fig. 7 and Fig. 13. The outputs $x_1(t)$ and $x_2(t)$ of the APF and the OSG-SOGI are obtained. The OSG input signal and parameters are the same for the simulation and the experimental part, where the input signal is a sinusoid with unity amplitude and frequency equal to the tuning frequency of the filter. A bandwidth of 4 Hz was set for the design of the OSGs. In the DSP, a fixed-point Q15 base was used for global calculations whereas a Q30 base was used for calculations of the filters.

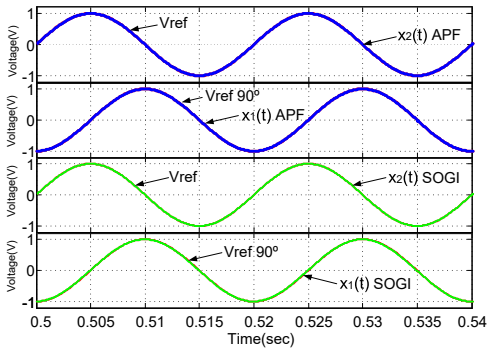

(a) Simulation.

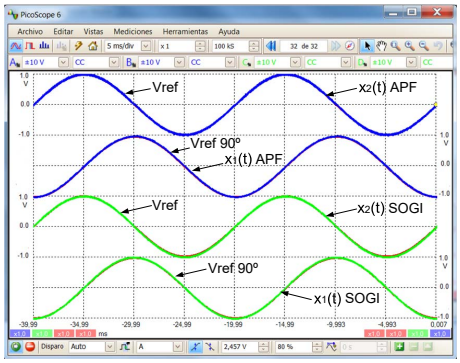

(b) DSP Implementation.

Fig. 21: $x_1(t)$ and $x_2(t)$ of the APF and the OSG-SOGI for a sampling frequency of 20 kHz and tuning frequency of 50 Hz.

In the experimental results obtained for the OSGs, channels A and B in blue are $x_2(t)$ and $x_1(t)$ of the APF with [1 V/div]; channels C and D in green are $x_2(t)$ and $x_1(t)$ of the SOGI with [1 V/div]. Corresponding reference signals (in red), an of the fundamental input signal on channels A and C and delayed signals 90 degrees with respect to this input signal on channels B and D, were added.

The results for a frequency of 50 Hz for the input signal and tuning, with a sampling frequency of 20 kHz, are presented in Fig. 21, where it is evidenced that both OSGs behave in accordance with the established, both in the simulation and in the DSP implementation. The outputs $x_1(t)$ and $x_2(t)$ follow their references and retain their waveform, and maintain the gain of 1, necessary condition for both OSGs operating as PLLs.

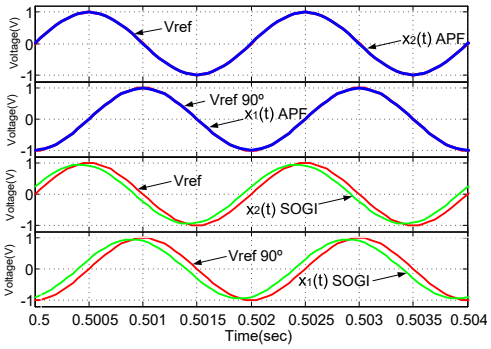

(a) Simulation.

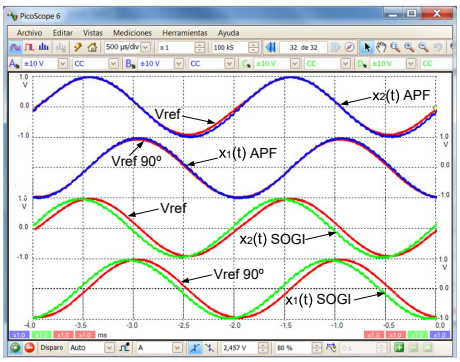

(b) DSP Implementation.

Fig. 22: $x_1(t)$ and $x_2(t)$ of the APF and the OSG-SOGI for a sampling frequency of 20 kHz and tuning frequency of 500 Hz.

The sampling frequency is kept at 20 kHz and the frequency of the input and tuning signal was increased to 500 Hz in Fig. 22 and 1000 Hz in Fig. 23. In the simulation for both tuning frequencies, the signals of the orthogonal system corresponding to the APF have a good follow-up of the reference signals with a gain of 1. The OSG-SOGI, loses its characteristics like OSG, with an advance of 0.0002 seconds, relative to the reference signals, which introduces a phase shift, as well as a decrease in the gain, which is not reaching 1.

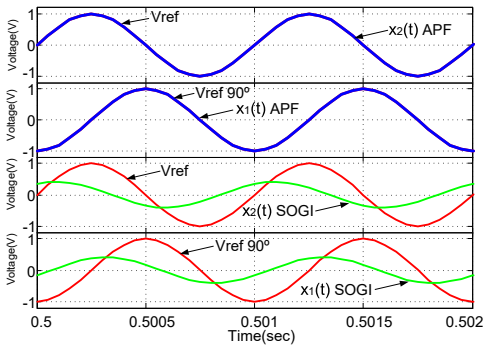

(a) Simulation.

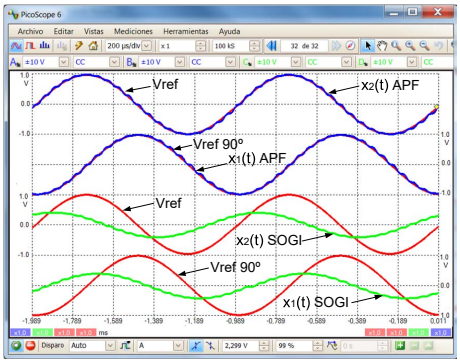

(b) DSP Implementation.

Fig. 23: $x_1(t)$ and $x_2(t)$ of the APF and the OSG-SOGI for a sampling frequency of 20 kHz and tuning frequency of 1000 Hz.

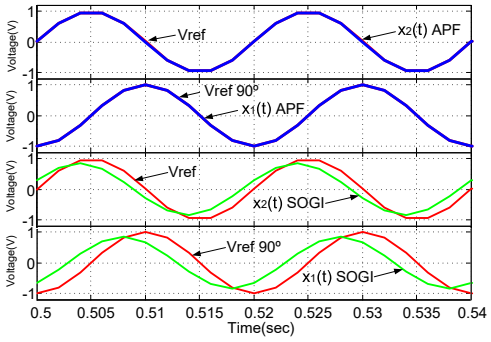

(a) Simulation.

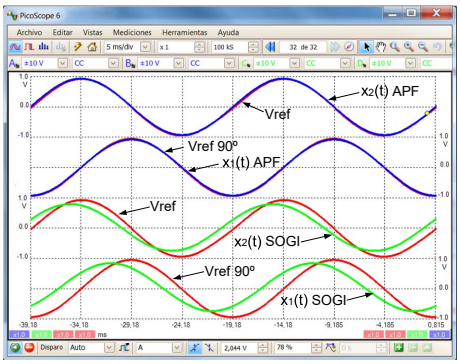

(b) DSP Implementation.

Fig. 24: $x_1(t)$ and $x_2(t)$ of the APF and the OSG-SOGI for a sampling frequency of 500 Hz and tuning frequency of 50 Hz.

In the implementation on a DSP, the responses of the APF are almost identical as in the simulation, there is a minimum advance of the signals, with respect to the reference signals, but not as pronounced as the case of OSG-SOGI, which maintains the same simulation behavior.

In Fig. 24, the outputs $x_1(t)$ and $x_2(t)$ are shown, for a different and extreme conditions, with a 50 Hz frequency of the signal input and tuning and with the sampling frequency lowered to 500 Hz. Both in the simulation and in the implementation in the DSP, the signals of the orthogonal system of the APF have a good follow-up of the reference signals with a gain of 1. In contrast, the OSG-SOGI signals are 0.0012 s ahead of the reference signals, which introduces a phase shift, as well as a 10 % decrease in gain, with respect to the input signals.

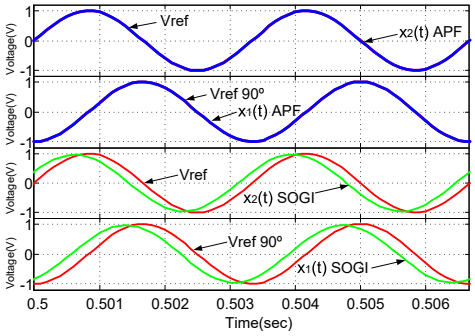

(a) Simulation.

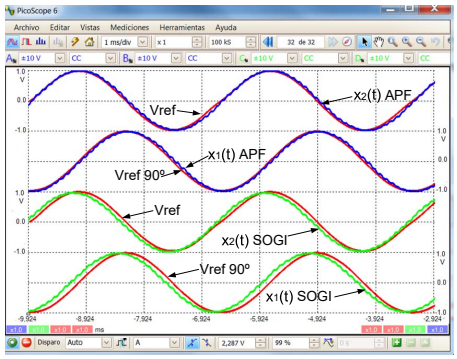

(b) DSP Implementation.

Fig. 25: $x_1(t)$ and $x_2(t)$ of the APF and the OSG-SOGI for a sampling frequency of 10 kHz and tuning frequency of 300 Hz.

In Fig. 25, the frequency of the input and tuning signal is increased to 300 Hz, with the sampling frequency at 10 kHz. The outputs of the APF remain the same as in the previous cases, maintaining their characteristics as OSG, which does not happen with the OSG-SOGI. The OSG-SOGI outputs continue to show poor tracking of the reference signals, with an advance of 0.0002 s, in the simulation and in the implementa-

tion in the DSP, although it maintains the gain of 1 in both cases.

6. Conclusion

This paper compared two different methods for generating the orthogonal quantity required for the PLL algorithm present in single-phase grid-connected inverter control. The analysis based on models of the state equations, showed that the method that uses the lattice APF exhibits better performance, although the results obtained with the SOGI structure are also acceptable.

A detailed mathematical analysis showed that these two orthogonal generators are equivalent and have an almost identical response in the range around the most common tuning frequency, i.e. 50 Hz, and also for sampling frequency values greater than 1 kHz. It was also demonstrated that the lattice APF is more stable since it retained its characteristics under all test conditions, although the tuning frequency was very high and the sampling frequency was very low, which does not occur with SOGI.

The parameters or coefficients of the matrix of the state equations of the lattice-based APF are more constant than those of the SOGI. The use of trigonometric functions to obtain these parameters ensures that they will always be in a minimum dynamic range of variation between -1 and $+1$. This is very suitable for applications using a fixed-point DSP. The obtained results showed a balance between good precision and resolution. The APF coefficients must not be scaled to enable their fitting within the dynamic range and processor's word length to allow their storage in the program memory. In this way, APF operation is almost identical to that specified in the design.

The theoretical evaluations were verified through extensive simulation and experimental studies. The study supports the conclusion that the lattice-based APF can provide the same functions in all applications where SOGI has been used so far as orthogonal generator, and also in others where tuning frequencies are higher or sampling frequencies are lower, as well as in the field of instrumentation, communications, analog electronics.

Most PLLs for three-phase applications, such as those presented in [12], have an OSG in their structure. This role can be fulfilled very well by the lattice-based APF, providing the advantages of working at higher tuning frequencies or lower sampling frequencies. Advantages that were verified in [50] when using the APF-PLL, guaranteeing fast dynamic response, good ripple filtering, easy implementation, low computation burden and a solution for harmonic components.

Author Contributions

J. B. encouraged L. B. to investigate about generators of an orthogonal system, starting from the Lattice structure to be used in a Phase Locked Loop (PLL) and to compare them with other algorithms. L. B. and J. B. conceived the original idea, the main conceptual ideas and the design of the study presented. They were in charge of directing and supervising project findings, overall planning, test scheme planning, and experiments. L. B. developed the formalism and the theoretical framework, performed the analytical calculations, planned and carried out the simulations. He wrote the manuscript with the support and input of N. A. and J. B. L. B. and N. A. carried out the implementation of the model and the experiments. They did almost all the technical details, numerical calculations, and measurements for the experiments. They processed and analyzed the experimental results. N. A. contributed to the design of the figures. All authors provided critical comments and helped shape, design and implement the research, contributed to the interpretation, analysis and discussion of the results, and to the writing of the final version of the manuscript.

References

[1] AREFIFAR, S. and Y. MOHAMED. Probabilistic Optimal Reactive Power Planning in Distribution Systems With Renewable Resources in Grid-Connected and Islanded Modes. *IEEE Transactions on Industrial Electronics*. 2014, vol. 61, iss. 11, pp. 5830–5839. ISSN 0278-0046. DOI:10.1109/TIE.2014.2308144.

[2] ZHOU, T.and B. FRANCOIS. Energy Management and Power Control of a Hybrid Active Wind Generator for Distributed Power Generation and Grid Integration. *IEEE Transactions on Industrial Electronics*. 2011, vol. 58, iss. 1, pp. 95–104. ISSN 0278-0046. DOI: 10.1109/TIE.2010.2046580.

[3] AWADALLAH, M. A. and B. VENKATESH. Energy Storage in Distribution System Planning and Operation: Current Status and Outstanding Challenges. *Canadian Journal of Electrical and Computer Engineering*. 2019, vol. 42, iss. 1, pp. 10–19. ISSN 0840-8688. DOI: 10.1109/CJECE.2018.2878321.

[4] ABOUDRAR, I., S. EL HANI, H. MEDIOUNI and A. AGHMADI. Modeling and Robust Control of a Grid Connected Direct Driven PMSG Wind Turbine By ADRC. *Advances in Electrical and Electronic Engineering*. 2018, vol. 16, iss. 4, pp. 402–413. ISSN 1804-3119. DOI: 10.15598/aeee.v16i4.2952.

[5] WANG, Y. F. and Y. W. LI. A Grid Fundamental and Harmonic Component Detection Method for Single-Phase Systems. *IEEE Transactions on Power Electronics*. 2013, vol. 28, iss. 5, pp. 2204–2213. ISSN 0885-8993. DOI: 10.1109/TPEL.2012.2214445.

[6] BOJOI, R. I., L. R. LIMONGI, D. ROIU and A. TENCONI. Enhanced Power Quality Control Strategy for Single-Phase Inverters in Distributed Generation Systems. *IEEE Transactions on Power Electronics* . 2011, vol. 26, iss. 3, pp. 798–806. ISSN 0885-8993. DOI: 10.1109/TPEL.2010.2103572.

[7] GHARTEMANI, M. K., S. A. KHAJEHODDIN, P. K. JAIN and A. BAKHSHAI. Problems of Startup and Phase Jumps in PLL Systems. *IEEE Transactions on Power Electronics*. 2012, vol. 27, iss. 4, pp. 1830–1838. ISSN 0885-8993. DOI: 10.1109/TPEL.2011.2169089.

[8] KARIMI-GHARTEMANI, M. K., M. MOJIRI, A. SAFAEE, J. WALSETH, S. A. KHAJEHODDIN, P. K. JAIN and A. BAKHSHAI. A New Phase-Locked Loop System for Three-Phase Applications. *IEEE Transactions on Power Electronics*. 2013, vol. 28, iss. 3, pp. 1208–1218. ISSN 0885-8993. DOI: 10.1109/TPEL.2012.2207967.

[9] AHMED, H. and M. E. H. BENBOUZID. Multiple Nonlinear Harmonic Oscillator-Based Frequency Estimation for Distorted Grid Voltage. *IEEE Transactions on Instrumentation and Measurement*. 2019, vol. 69, iss. 6, pp. 2817–2825. ISSN 0018-9456. DOI: 10.1109/TIM.2019.2931065.

[10] TAUL, M. G., X. WANG, P. DAVARI and F. BLAABJERG. An Overview of Assessment Methods for Synchronization Stability of Grid-Connected Converters Under Severe Symmetrical Grid Faults. *IEEE Transactions on Power Electronics*. 2019, vol. 34, iss. 10, pp. 9655–9670. ISSN 0885-8993. DOI: 10.1109/TPEL.2019.2892142.

[11] AHMED, H., M. BENBOUZID, M. AHSAN, A. ALBARBAR and M. SHAHJALAL. Frequency Adaptive Parameter Estimation of Unbalanced and Distorted Power Grid. *IEEE Access*. 2020, vol. 8, iss. 1, pp. 8512–8519. ISSN 2169-3536. DOI: 10.1109/ACCESS.2020.2964058.

[12] MERAL, M. E. and D. CELIK. A comprehensive survey on control strategies of distributed generation power systems under normal and abnormal conditions. *Annual Reviews in Control*. 2019, vol. 47, iss. 1, pp. 112–132. ISSN 1367-5788. DOI: 10.1016/j.arcontrol.2018.11.003.

[13] GONZALEZ-ESPIN, F., G. GARCERA, I. PATRAO and E. FIGUERES. An Adaptive Control System for Three-Phase Photovoltaic Inverters Working in a Polluted and Variable Frequency Electric Grid. *IEEE Transactions on Power Electronics*. 2012, vol. 27, iss. 10, pp. 4248–4261. ISSN 0885-8993. DOI: 10.1109/TPEL.2012.2191623.

[14] REZA, M. S., F. SADEQUE, M. M. HOSSAIN, A. M. Y. M. GHIAS and V. G. AGELIDIS. Three-Phase PLL for Grid-Connected Power Converters Under Both Amplitude and Phase Unbalanced Conditions. *IEEE Transactions on Industrial Electronics*. 2019, vol. 66, iss. 11, pp. 8881–8891. ISSN 0278-0046. DOI: 10.1109/TIE.2019.2893857.

[15] CIOBOTARU, M., R. TEODORESCU and F. BLAABJERG. A new single-phase PLL structure based on second order generalized integrator. In: *2006 37th IEEE Power Electronics Specialists Conference*. Jeju: IEEE, 2006, pp. 1–6. ISBN 0-7803-9716-9. DOI: 10.1109/PESC.2006.1711988.

[16] GOLESTAN, S., J. M. GUERRERO and J. C. VASQUEZ. Single-Phase PLLs: A Review of Recent Advances. *IEEE Transactions on Power Electronics*. 2017, vol. 32, iss. 12, pp. 9013–9030. ISSN 0885-8993. DOI: 10.1109/TPEL.2017.2653861.

[17] GOLESTAN, S., J. M. GUERRERO, A. ABUSORRAH, M. M. AL-HINDAWI and Y. AL-TURKI. An Adaptive Quadrature Signal Generation-Based Single-Phase Phase-Locked Loop for Grid-Connected Applications. *IEEE Transactions on Industrial Electronics*. 2017, vol. 64, iss. 4, pp. 2848–2854. ISSN 0278-0046. DOI: 10.1109/TIE.2016.2555280.

[18] KARIMI-GHARTEMANI, M., S. A. KHAJEHODDIN, P. K. JAIN, A. BAKHSHAI and M. MOJIRI. Addressing DC Component in PLL and Notch Filter Algorithms. *IEEE Transactions on Power Electronics*. 2012, vol. 27, iss. 1, pp. 78–86. ISSN 0885-8993. DOI: 10.1109/TPEL.2011.2158238.

[19] NAYAK, S., S. GURUNATH and N. RAJASEKAR. Advanced single-phase inverse park PLL with tuning of PI controller for improving stability of grid utility using soft computing technique. In: *2016 Online International Conference on Green Engineering and Technologies (IC-GET)*. Coimbatore: IEEE, 2016, pp. 1–5. ISBN 978-1-5090-4557-0. DOI: 10.1109/GET.2016.7916732.

[20] LIU, B., M. AN, H. WANG, Y. CHEN, Z. ZHANG, C. XU, S. SONG and Z. LV.

A Simple Approach to Reject DC Offset for Single-Phase Synchronous Reference Frame PLL in Grid-Tied Converters. *IEEE Access*. 2020, vol. 8, iss.1, pp. 112297–112308. ISSN 2169-3536. DOI: 10.1109/ACCESS.2020.3003009.

[21] CIOBOTARU, M., R. TEODORESCU and F. BLAABJERG. Improved PLL structures for single-phase grid inverters. *International Conference on Power Electronics and Intelligent Control for Energy Conservation (PELINCEC'05)*. Warsaw: Warsaw University of Technology, 2005, pp. 1–6.

[22] SI, Y., Y. LIU, C. LIU, Z. ZHANG and Q. LEI. Reactive Power Injection and SOGI Based Active Anti-Islanding Protection Method. In: *2019 IEEE Energy Conversion Congress and Exposition (ECCE)*. Baltimore: IEEE, 2019, pp. 2637–2642. ISSN: 2329-3748. DOI: 10.1109/ECCE.2019.8912539.

[23] LUBURA, S., M. SOJA, S.-A. LALE and M. IKIC. Single-phase phase locked loop with DC offset and noise rejection for photovoltaic inverters. *IET Power Electronics*. 2014, vol. 7, iss. 9, pp. 2288–2299. ISSN 1755-4535. DOI: 10.1049/iet-pel.2013.0413.

[24] ECHCHAACHOUAI, A., S. EL HANI, A. HAMMOUCH and I. ABOUDRAR. A Two-Level Sensorless MPPT Strategy Using SRF-PLL on a PMSG Wind Energy Conversion System. *Advances in Electrical and Electronic Engineering*. 2017, vol. 15, iss. 3, pp. 383–390. ISSN 1804-3119. DOI: 10.15598/aeee.v15i3.2215.

[25] STOJIC, D., N. GEORGIJEVIC, M. RIVERA and S. MILIC. Novel orthogonal signal generator for single phase PLL applications. *IET Power Electronics*. 2018, vol. 11, iss. 3, pp. 427–433. ISSN 1755-4535. DOI: 10.1049/iet-pel.2017.0458.

[26] HAN, Y., M. LUO, X. ZHAO, J. M. GUERRERO and L. XU. Comparative Performance Evaluation of Orthogonal-Signal-Generators-Based Single-Phase PLL Algorithms—A Survey. *IEEE Transactions on Power Electronics*. 2016, vol. 31, iss. 5, pp. 3932–3944. ISSN 1941-0107. DOI: 10.1109/TPEL.2015.2466631.

[27] SUBRAMANIAN, C. and R. KANAGARAJ. Single-Phase Grid Voltage Attributes Tracking for the Control of Grid Power Converters. *IEEE Journal of Emerging and Selected Topics in Power Electronics*. 2014, vol. 2, iss. 4, pp. 1041–1048. ISSN 2168-6785. DOI: 10.1109/JESTPE.2014.2341045.

[28] ELRAYYAH, A., Y. SOZER and M. ELBULUK. Robust phase locked-loop algorithm for single-phase utility-interactive inverters. *IET Power Electronics*. 2014, vol. 7, iss. 5, pp. 1064–1072. ISSN 1755-4535. DOI: 10.1049/iet-pel.2013.0351.

[29] FOYEN, S., C. ZHANG, O. FOSSO and M. MOLINAS. Frequency Domain Modelling for Assessment of Hilbert and SOGI Based Single-Phase Synchronisation. In: *IECON 2019 - 45th Annual Conference of the IEEE Industrial Electronics Society*. Lisbon: IEEE, 2019, pp. 1780–1785. ISBN 978-1-7281-4878-6. DOI: 10.1109/IECON.2019.8926656.

[30] ZHANG, C., X. WANG, F. BLAABJERG, W. WANG and C. LIU. The influence of phase-locked loop on the stability of single-phase grid-connected inverter. In: *2015 IEEE Energy Conversion Congress and Exposition (ECCE)*. Montreal: IEEE, 2015, pp. 4737–4744. ISBN 978-1-4673-7151-3. DOI: 10.1109/ECCE.2015.7310329.

[31] HWANG, S., L. LIU, H. LI, and J. KIM. DC Offset Error Compensation for Synchronous Reference Frame PLL in Single-Phase Grid-Connected Converters. *IEEE Transactions on Power Electronics*. 2012, vol. 27, iss. 8, pp. 3467–3471. ISSN 0885-8993. DOI: 10.1109/TPEL.2012.2190425.

[32] MERAL, M. E. and D. CELIK. Benchmarking simulation and theory of various PLLs produce orthogonal signals under abnormal electric grid conditions. *Electrical Engineering*. 2018, vol. 100, iss. 3, pp. 1805–1817. ISSN 1432-0487. DOI: 10.1007/s00202-017-0660-x.

[33] AHMED, H., S. BIRICIK and M. BENBOUZID. Low-pass filtering or gain tuning free simple dc offset rejection technique for single and three-phase systems. *Electric Power Systems Research*. 2020, vol. 186, iss. 1. pp. 1–10. ISSN 0378-7796. DOI: 10.1016/J.EPSR.2020.106422.

[34] AHMED, H. and M. BENBOUZID. On the enhancement of generalized integrator-based adaptive filter dynamic tuning range. *IEEE Transactions on Instrumentation and Measurement*. 2020, vol. 69, iss. 10, pp. 7449–7457. ISSN 0018-9456. DOI: 10.1109/TIM.2020.2982232.

[35] AHMED, H. and M. BENBOUZID. Demodulation type single-phase PLL with DC offset rejection. *Electronics Letters*. 2020, vol. 56, iss. 7, pp. 344–347. ISSN 0013-5194. DOI: 10.1049/EL.2019.3718.

[36] REZA, M. S., M. CIOBOTARU and V. G. AGELIDIS. Accurate Estimation of Single-Phase Grid Voltage Parameters Under Distorted Conditions.

IEEE Transactions on Power Delivery. 2014, vol. 29, iss. 3, pp. 1138–1146. ISSN 0885-8977. DOI: 10.1109/TPWRD.2014.2303482.

[37] RODRIGUEZ, F. J., E. BUENO, M. AREDES, L. G. B. ROLIM, F. A. S. NEVES and M. C. CAVALCANTI. Discrete-time implementation of second order generalized integrators for grid converters. In: *2008 34th Annual Conference of IEEE Industrial Electronics*. Orlando: IEEE, 2008, pp. 176–181. ISBN 978-1-4244-1767-4. DOI: 10.1109/IECON.2008.4757948.

[38] TAGHIZADEH, S., M. J. HOSSAIN and J. LU. Enhanced orthogonal signal generator for a single-phase grid-connected converter. *IET Power Electronics*. 2018, vol. 11, iss. 15, pp. 2563–2572. ISSN 1755-4535. DOI: 10.1049/iet-pel.2018.5253.

[39] MATAS, J., H. MARTIN, J. DE LA HOZ, A. ABUSORRAH, Y. AL-TURKI and H. AL-SHAEIKH. A New THD Measurement Method With Small Computational Burden Using a SOGI-FLL Grid Monitoring System. *IEEE Transactions on Power Electronics*. 2020, vol. 35, iss. 6, pp. 5797–5811. ISSN 1941-0107. DOI: 10.1109/TPEL.2019.2953926.

[40] SHAH, S., P. KORALEWICZ, V. GEVORGIAN and L. PARSA. Small-Signal Modeling and Design of Phase-Locked Loops Using Harmonic Signal-Flow Graphs. *IEEE Transactions on Energy Conversion*. 2020, vol. 35, iss. 2, pp. 600–610. ISSN 0885-8969. DOI: 10.1109/TEC.2019.2954112.

[41] AHMED, H. and M. E. H. BENBOUZID. Simplified second-order generalized integrator-frequency-locked loop. *Advances in Electrical and Electronic Engineering*. 2019, vol. 17, iss. 4, pp. 405–412. ISSN 1804-3119. DOI:10.15598/aeee.v17i4.3540.

[42] XU, R., T. LAN, H. YIN, X. WU and Y. LAN. A Novel Three-Phase Phase-Locked Loop Based on DSOGI and Adaptive Observer Algorithm. In: *2019 4th IEEE Workshop on the Electronic Grid (eGRID)*. Xiamen: IEEE, 2019, pp. 1–5. ISBN: 978-1-7281-5704-7. DOI: 10.1109/eGRID48402.2019.9092744.

[43] RODRIGUEZ, P., A. LUNA, I. CANDELA, MUJAL, R. TEODORESCU and F. BLAABJERG. Multiresonant Frequency-Locked Loop for Grid Synchronization of Power Converters Under Distorted Grid Conditions. *IEEE Transactions on Industrial Electronics*. 2011, vol. 58, iss. 1, pp. 127–138. ISSN 0278-0046. DOI: 10.1109/TIE.2010.2042420.

[44] MERAL, M. E. and D. CELIK. DSOGI-PLL Based Power Control Method to Mitigate Control Errors Under Disturbances of Grid Connected Hybrid Renewable Power Systems. *Advances in Electrical and Electronic Engineering*. 2018, vol. 16, iss. 1, pp. 81–91. ISSN 1804-3119. DOI: 10.15598/aeee.v16i1.2485.

[45] HOGAN, D. J., F. J. GONZALEZ-ESPIN, J. G. HAYES, G. LIGHTBODY and R. FOLEY. An Adaptive Digital-Control Scheme for Improved Active Power Filtering Under Distorted Grid Conditions. *IEEE Transactions on Industrial Electronics*. 2018, vol. 65, iss. 2, pp. 988–999. ISSN 0278-0046. DOI: 10.1109/TIE.2017.2726992.

[46] RIVAS, H. A. and J. BERGAS. Frequency Determination in a Single-Phase Voltage Signal using Adaptative Notch Filters. In: *2007 9th International Conference on Electrical Power Quality and Utilisation*. Barcelona: IEEE, 2007, pp. 1–7. ISSN 2150-6647. DOI: 10.1109/EPQU.2007.4424151.

[47] REGALIA, P. A., S. K. MITRA and P. P. VAIDYANATHAN. The digital all-pass filter: a versatile signal processing building block. *Proceedings of the IEEE*. 1988, vol. 76, iss. 1, pp. 19–37. ISSN 0018-9219. DOI: 10.1109/5.3286.

[48] GONZALEZ-ESPIN, F., I. PATRAO, E. FIGUERES and G. GARCERA. An Adaptive Digital Control Technique for Improved Performance of Grid Connected Inverters. *IEEE Transactions on Industrial Informatics*. 2013, vol. 9, iss. 2, pp. 708–718. ISSN 1551-3203. DOI: 10.1109/TII.2012.2225437.

[49] REGALIA, P. A. An improved lattice-based adaptive IIR notch filter. *IEEE Transactions on Signal Processing*. 1991, vol. 39, iss. 9, pp. 2124–2128. ISSN 1053-587X. DOI: 10.1109/78.134453.

[50] BELANDRIA, L. and J. BERGAS-JANE. Single-Phase PLL based on an Adaptive Notch Filter. *Advances in Electrical and Electronic Engineering*. 2020, vol. 18, iss. 3, pp. 169–179. ISSN 1804-3119. DOI: 10.15598/aeee.v18i3.3807.

About Authors

Luciano Emilio BELANDRIA was born in Merida, Venezuela, in 1969. He received the B.S. degree in Electrical Engineering from the University of Los Andes (ULA), Merida, Venezuela in 1995 and the Ph.D. degree in Electrical engineering from the Polytechnic University of Catalonia (UPC), Barcelona, Spain, in 2015. Since 2001, he has been a Professor with the

Electronics Engineering Department, the University of Tachira (UNET), San Cristobal, Venezuela. His research interest areas are power electronics, digital motor control, renewable energy, distributed energy resources, voltage and frequency control, and neural networks.

Nancy Alejandra AGUDELO was born in San Cristóbal, Venezuela, in 1969. She received the B.S. degree in Electrical Engineering from the University of Los Andes (ULA), Merida, Venezuela in 1996 and the Ph.D. degree in Electrical engineering from the Polytechnic University of Catalonia (UPC), Barcelona, Spain, in 2015. Since 2001, she has been a Professor with the Electronics Engineering Department, the University National Experimental of Táchira (UNET), San Cristobal, Venezuela. Her research interest areas are energy efficiency, energy audits using standard 50001, and electrical installations.

Joan BERGAS-JANE was born in Manresa, Spain, in 1970. He received the B.S. degree in industrial engineering and the Ph.D. degree in engineering from the Polytechnic University of Catalonia (UPC), Barcelona, Spain, in 1992 and 2000, respectively. Since 2002, he has been Assistant Professor in the Electrical Engineering Department, Polytechnic University of Catalonia. His research interest lies in the areas of power system quality, power electronics, and digital motor control.

Appendix A Nomenclature

PCC	Point of Common Coupling
OSG	Orthogonal Signal Generator
PLL	Phase-Locked Loop
$SOGI$	Second-Order Generalized Integrator
θ	Utility phase-angle of the input signal
ω_0	Notch frequency
BW	Band width of the filter
B	Band pass
f_s	Sampling frequency
$u(n)$	Input signal
$y(n)$	Output filtered
$x_1(n)$, $x_2(n)$	Orthogonal components
V_{ac}	Grid voltage
V_d	d-axis voltage
V_q	q-axis voltage
V_α	α-axis voltage output of the OSG
V_β	β-axis voltage output of the OSG
V_{RMS}	Root Mean Square Voltage